Journal of Biomolecular NMR, **14:** 241–252, 1999.
KLUWER/ESCOM

^{13}C spin relaxation measurements in RNA: Sensitivity and resolution improvement using spin-state selective correlation experiments

Jérôme Boisbouvier, Bernhard Brutscher, Jean-Pierre Simorre & Dominique Marion*
Institut de Biologie Structurale Jean-Pierre Ebel, C.N.R.S.-C.E.A., 41 rue Jules Horowitz, F-38027 Grenoble Cedex, France

Received 15 March 1999; Accepted 3 May 1999

Key words: ^{13}C relaxation, conformational exchange, cross correlation, CSA, nucleic acids, TROSY

Abstract

A set of new NMR pulse sequences has been designed for the measurement of ^{13}C relaxation rate constants in RNA and DNA bases: the spin-lattice relaxation rate constant $R(C_z)$, the spin-spin relaxation rate constant $R(C_+)$, and the CSA-dipolar cross-correlated relaxation rate constant $\Gamma^{xy}_{C,CH}$. The use of spin-state selective correlation techniques provides increased sensitivity and spectral resolution. Sensitivity optimised C-C filters are included in the pulse schemes for the suppression of signals originating from undesired carbon isotopomers. The experiments are applied to a 15% ^{13}C-labelled 33-mer RNA–theophylline complex. The measured $R(C_+)/\Gamma^{xy}_{C,CH}$ ratios indicate that ^{13}C CSA tensors do not vary significantly for the same type of carbon (C_2, C_6, C_8), but that they differ from one type to another. In addition, conformational exchange effects in the RNA bases are detected as a change in the relaxation decay of the narrow ^{13}C doublet component when varying the spacing of a CPMG pulse train. This new approach allows the detection of small exchange effects with a higher precision compared to conventional techniques.

Introduction

Recent advances in heteronuclear NMR and isotopic enrichment methods have enabled ^{15}N and ^{13}C spin relaxation to become widely used for the study of the dynamical properties of biological molecules. As isotope labelling became available for proteins earlier than for oligonucleotides, a large number of proton-detected heteronuclear correlation experiments have been devised to study local motions in proteins over a wide range of time scales. Most NMR studies of protein dynamics have focused on ^{15}N relaxation measurements, where spin relaxation is mainly caused by the dipole–dipole (DD) interaction with the directly attached proton and the ^{15}N chemical shift anisotropy (CSA). Typically, the ^{15}N spin-lattice $R(N_z)$ and spin-spin $R(N_+)$ relaxation rate constants and the ^{15}N-{^{1}H} NOE are measured using a series of modified HSQC experiments (Kay et al., 1989). As the CSA interaction is to a good approximation axially symmetric and collinear to the dipolar interaction, these relaxation data can be interpreted in terms of angular fluctuations of the internuclear N-H vector.

This strategy cannot be easily transferred to DNA or RNA oligomers because of their different chemical structure. So far only few relaxation studies on nucleic acids have been reported. ^{15}N spin relaxation measurements are limited to a few sites in the molecule because the base nitrogens are either attached to fast exchanging imino or amino protons or not directly bound to any proton, although some information on molecular dynamics has been recently obtained from ^{15}N relaxation data measured for two uracil N_3 and five guanine N_1 nitrogens in a 14-mer RNA hairpin (Akke et al., 1997). The use of ^{13}C as a relaxation probe is hampered by the presence of complicated carbon spin-coupling topologies and the large and fully anisotropic ^{13}C CSA tensors. Most

*To whom correspondence should be addressed. E-mail: marion@rmn.ibs.fr

information has been obtained from ^{13}C relaxation measurements on site-specifically ^{13}C enriched molecules, for example labelled on the $C_{1'}$ (Paquet et al., 1996) or C_6 (Williamson and Boxer, 1989) position, or on natural abundance samples (Borer et al., 1994; Spielmann, 1998). Only the latter approach, however, allows a comprehensive investigation of local molecular dynamics in the different sugars and bases. It has however been shown for the case of protein sidechains (Wand et al., 1995), and very recently also for RNA purine nucleotides (Kojima et al., 1998), that low level random fractional enrichment at all carbon sites can considerably reduce the problems associated with homonuclear ^{13}C couplings and increase the overall sensitivity of the relaxation experiments with respect to natural abundance samples. Alternatively, constant-time frequency labelling, selective spin decoupling, and selective spin locking techniques have been proposed to record ^{13}C relaxation experiments on fully ^{13}C-labelled molecules. While these techniques can partially resolve problems associated with scalar J_{CC} coupling evolution, they do not refocus ^{13}C-^{13}C dipolar contributions to spin relaxation, which increase with molecular weight (Yamazaki et al., 1994).

The major problems for the accurate determination of ^{13}C relaxation rate constants in fractional ^{13}C-labelled RNA remain the poor sensitivity and spectral resolution of ^{1}H-^{13}C correlation spectra due to the fast transverse relaxation of both ^{1}H and ^{13}C. We have recently demonstrated that spin-state selective ^{13}C frequency editing greatly improves both the resolution and the sensitivity of ^{1}H-^{13}C correlation spectra of RNA (Brutscher et al., 1998). Because of cross-correlation between ^{13}C CSA and ^{1}H-^{13}C dipolar interactions, the two lines of a peak doublet in a scalar-coupled two-spin system exhibit different line widths. In other words, the relaxation properties of ^{13}C depend on the spin state of the scalar coupled ^{1}H. Several experimental techniques have been proposed recently to achieve spin-state selection by means of a train of non-selective rf pulses: TROSY (Pervushin et al., 1997, 1998b), IPAP (Ottiger et al., 1998) or S^3E (Meissner et al., 1997). Selection of only the narrow line by the pulse sequence yields a gain in spectral resolution and in favourable cases also yields an increase in sensitivity. In addition, the ^{1}H and ^{13}C steady-state magnetisations can be simultaneously transferred into a detectable NMR signal by these pulse sequences, thus partially compensating the factor of two signal loss due to the line selection. This new methodology is especially attractive for nuclei with large chemical shielding anisotropies in molecules with a low proton density (inefficient ^{1}H spin-lattice relaxation). This is the case for the base carbons in nucleic acids, where resolution enhancement factors of up to five are obtained at currently available magnetic field strengths (Brutscher et al., 1998).

Here we report new experiments for measuring ^{13}C relaxation rate constants in the bases of randomly ^{13}C-labelled RNAs. A first pulse scheme allows the measurement of the auto-correlated relaxation parameters $R(C_+)$ and $R(C_z)$, a second one has been designed to measure the CSA-dipolar cross-correlated relaxation rate constant $\Gamma^{xy}_{C,CH}$ from the differential relaxation behaviour of the two ^{13}C doublet lines. Furthermore, the average relaxation rate of the two doublet lines provides a valuable estimate of the spin-spin relaxation rate constant $R(C_+)$. All pulse sequences include the features of spin-state selective ^{13}C frequency editing and allow the combined use of ^{1}H and ^{13}C steady-state magnetisations. Additional filter sequences, required for the selection of specific carbon-carbon isotopomers, have been included and signal loss during the filter is minimised by the use of spin-state selective techniques. All relaxation rate constants are obtained from the mono-exponential intensity decay of well-resolved cross peaks recorded in a series of 2D experiments. On the basis of the measured relaxation rate constants a few conclusions can be drawn on the magnitude of ^{13}C CSA tensors in RNA oligonucleotides. Additional information on conformational exchange processes in the RNA is obtained by sampling the relaxation decay of the slowly relaxing ^{13}C doublet line with varying CPMG inter-pulse delays.

Theoretical background

Considering an isolated scalar coupled two-spin system ^{13}C-^{1}H, analytical expressions can be derived for the spin dynamics in Liouville space (Goldman, 1984). During a free evolution period and neglecting chemical shift evolution, the master equation, which governs the spin dynamics, can be written in the basis of the shift-operators $C_+ = C_x + iC_y$ and $2C_+H_z = 2C_xH_z + i2C_yH_z$ as

$$\frac{d}{dt}\begin{pmatrix} C_+ \\ 2C_+H_z \end{pmatrix} = -L\begin{pmatrix} C_+ \\ 2C_+H_z \end{pmatrix} \qquad (1)$$

with

$$L = \begin{pmatrix} R(C_+) & \Gamma^{xy}_{C,CH} + i\pi J_{CH} \\ \Gamma^{xy}_{C,CH} + i\pi J_{CH} & R(C_+H_z) \end{pmatrix}$$

with the auto-correlated relaxation rate constants $R(C_+)$, $R(C_+H_z)$, the CSA-dipolar cross-correlated relaxation rate constant $\Gamma^{xy}_{C,CH}$, and the scalar one-bond coupling constant J_{CH}.

For the discussion of the pulse sequence of Figure 1C it is more convenient to transform Equation 1 in the basis of the single-transition operators $C_+^{(\alpha)} = 1/2(C_+ - 2C_+H_z)$ and $C_+^{(\beta)} = 1/2(C_+ + 2C_+H_z)$, where the superscripts (α) and (β) indicate the spin-state of the ^{1}H following a commonly used sign convention (Cavanagh et al., 1996):

$$\frac{d}{dt}\begin{pmatrix} C_+^{(\alpha)} \\ C_+^{(\beta)} \end{pmatrix} = -L' \begin{pmatrix} C_+^{(\alpha)} \\ C_+^{(\beta)} \end{pmatrix} \tag{2}$$

with

$$L' = \begin{pmatrix} -i\pi J_{CH} + \overline{R}_+ - \Gamma^{xy}_{C,CH} & \Delta R_+ \\ \Delta R_+ & i\pi J_{CH} + \overline{R}_+ + \Gamma^{xy}_{C,CH} \end{pmatrix}$$

with $\overline{R}_+ = (R(C_+) + R(C_+H_z))/2$ and $\Delta R_+ = (R(C_+) - R(C_+H_z))/2$. The off-diagonal elements ΔR_+ can be neglected if $\sqrt{(\pi J_{CH})^2 + (\Gamma^{xy}_{C,CH})^2} \gg \Delta R_+$. In this case, relaxation of the two ^{13}C doublet lines described by the single-transition operators $C_+^{(\alpha)}$ and $C_+^{(\beta)}$ is mono-exponential.

Spin relaxation in the ^{13}C-^{1}H system is governed by the ^{13}C CSA and the ^{13}C-^{1}H dipolar interactions. In the following we will assume isotropic molecular tumbling and isotropic local motions. In this case the different relaxation rate constants can be expressed in terms of the same power spectral density function $J(\omega)$ of the molecular motion:

$$\begin{aligned} R(C_+H_z) = {} & \frac{1}{8}\xi^2_{DD}\{4J(0) + J(\omega_H - \omega_C) \\ & + 3J(\omega_C) + 6J(\omega_H + \omega_C)\} \\ & + \frac{1}{18}(\overline{\Delta\sigma})^2\omega_C^2\{4J(0) + 3J(\omega_C)\} + R_{ex} \end{aligned} \tag{3}$$

$$R(C_+) = R(C_+H_z) + \frac{3}{4}\xi^2_{DD}J(\omega_H) \tag{4}$$

$$\Gamma^{xy}_{C,CH} = -\frac{1}{6}\xi_{DD}\Delta\sigma^*\omega_C\{4J(0) + 3J(\omega_C)\} \tag{5}$$

with the dipolar constant

$$\xi_{DD} = \frac{\mu_o}{4\pi}\frac{\gamma_C\gamma_H}{\langle r^3_{C\text{-}H}\rangle}\frac{h}{2\pi},$$

and ^{13}C Larmor frequency $\omega_C = \gamma_C B_0$. γ_C and γ_H are the gyromagnetic ratios of ^{13}C and ^{1}H, h is Planck's constant, μ_o is the magnetic field constant, and $r_{C\text{-}H}$ is the C-H bond length. The ^{13}C CSA is described by the parameters $\overline{\Delta\sigma} = \sqrt{\sigma_x^2 + \sigma_y^2 - \sigma_x.\sigma_y}$ and $\Delta\sigma^* = P_2(\cos\theta^{xd})\sigma_x + P_2(\cos\theta^{yd})\sigma_y$, with $\sigma_x = \sigma_{xx} - \sigma_{zz}$ and $\sigma_y = \sigma_{yy} - \sigma_{zz}$. σ_{xx}, σ_{yy}, σ_{zz} are the principal values of the CSA tensor, θ^{xd} and θ^{yd} are the angles between the internuclear ^{13}C-^{1}H vector and the principal axes x and y of the CSA tensor, and $P_2(x)$ is the second order Legendre polynomial. $J(\omega)$ is normalized so that $J(0) = 2\tau_c/5$ for an isotropically tumbling rigid molecule with correlation time τ_c. The additional term R_{ex} takes into account conformational exchange contributions resulting from fluctuations in the micro- to millisecond time-scale range.

The dependence of the relaxation rate constant $R(C_z)$ on the power spectral density function is given by

$$\begin{aligned} R(C_z) = {} & \frac{1}{4}\xi^2_{DD}\{J(\omega_H - \omega_C) \\ & + 3J(\omega_C) + 6J(\omega_H + \omega_C)\} \\ & + \frac{1}{3}(\overline{\Delta\sigma})^2\omega_C^2 J(\omega_C) \end{aligned} \tag{6}$$

All measured relaxation rate constants depend in a complex manner on the spectral density of the molecular motion sampled at several characteristic frequencies, the ^{13}C CSA tensor and some geometrical parameters (Equations 3–6). An elegant way to separate the dynamical contributions from the CSA and the geometrical parameters consists in looking at the ratio $R(C_+)/\Gamma^{xy}_{C,CH}$. In the case of biological macromolecules at high magnetic fields, the high frequency terms of the power spectral density function $J(\omega_H)$, $J(\omega_H - \omega_C)$, and $J(\omega_H + \omega_C)$ are small compared to $J(0)$ and $J(\omega_C)$ and can be safely neglected. In this case, both the transverse relaxation rate constant $R(C_+)$ and the cross-correlated relaxation rate constant $\Gamma^{xy}_{C,CH}$ are proportional to $(4J(0) + 3J(\omega_C))$. Therefore, for spin systems devoid of any conformational exchange contribution R_{ex}, the $R(C_+)/\Gamma^{xy}_{C,CH}$ ratio becomes independent of the molecular motion (Fushman and Cowburn, 1998):

$$\frac{R(C_+)}{\Gamma^{xy}_{C,CH}} = \frac{9\xi^2_{DD} + 4\gamma_C^2 B_0^2\overline{\Delta\sigma}^2}{12\xi_{DD}\gamma_C B_0\Delta\sigma^*} \tag{7}$$

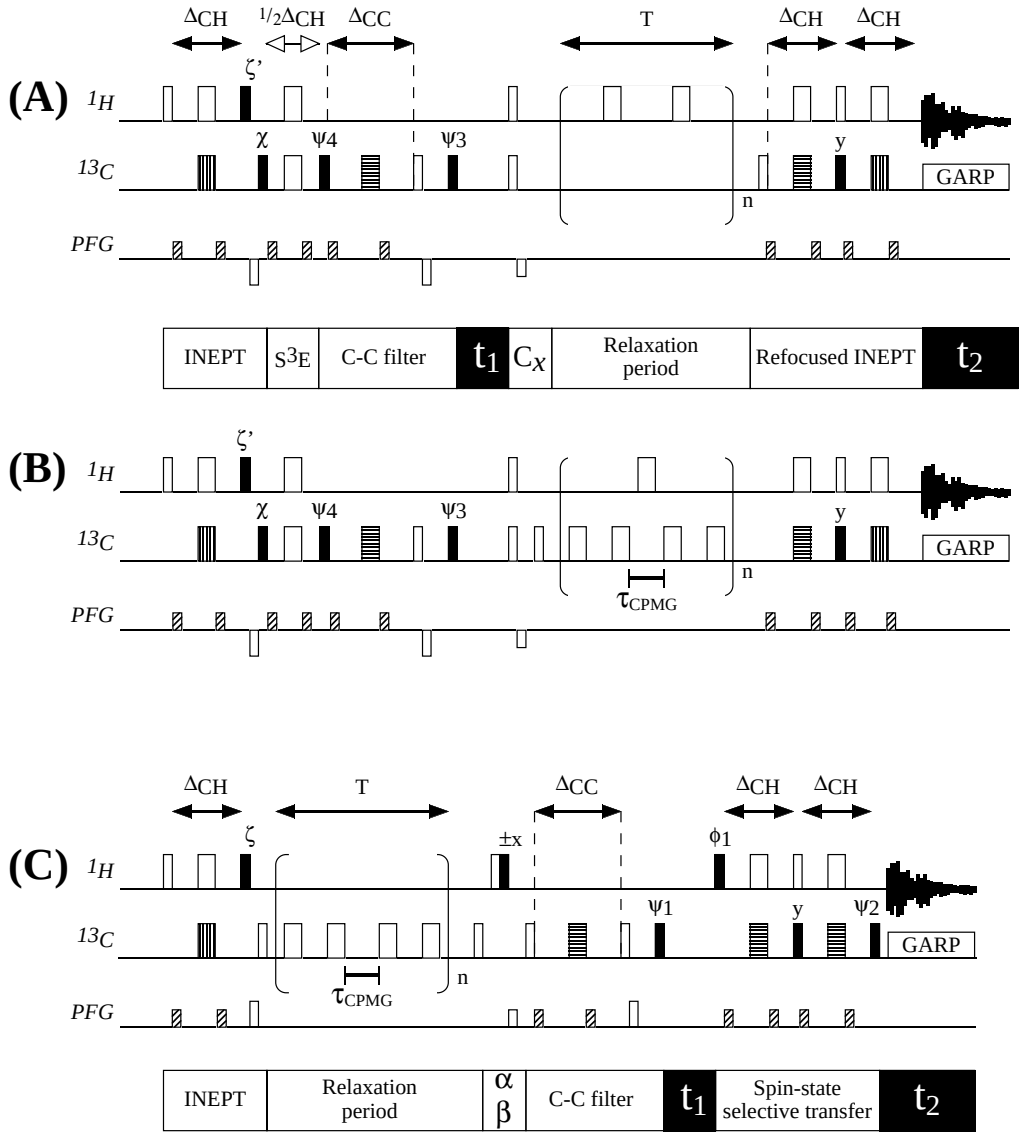

Figure 1. NMR experiments for the measurement of ^{13}C spin relaxation rate constants in the bases of nucleic acids. The pulse sequences have been designed to measure the relaxation rates of C_z(A) and C_+(B), and of the individual line components $C_+^{(\alpha)}$ and $C_+^{(\beta)}$ of the ^{13}C doublet (C). The underlying concept is illustrated by a sequence of NMR building blocks. Thin and wide bars represent 90° and 180° rf pulses, respectively. Composite ^{13}C 180° pulses are used for broadband spin inversion (90°_x, 240°_y, 90°_x) and refocusing (59.4°_x, 298°_{-x}, 59.4°_x). Composite inversion pulses are indicated by vertically dashed bars, refocusing pulses by horizontally dashed bars. Open bars indicate rf pulses applied along the x-axis, while black bars correspond to other constant or cycled phases. The transfer and filter delays were set to $\Delta_{CH} = 1/2J_{CH} = 2.6$ ms and $\Delta_{CC} = 1/2J_{CH} = 7.5$ ms. ^{13}C decoupling during ^{1}H detection is achieved using GARP (Shaka et al., 1985) with an rf field strength of $|\gamma B_1|/2\pi = 3$ kHz. Pulsed field gradients were applied along the z-axis with a strength of approximately 70 G/cm. To avoid creation of echoes, all purging gradients or pairs of gradients (on either side of 180° pulses) were set to unequal lengths ranging from 100 to 600 μs with a recovery delay of 100 μs. Off-resonance rf irradiation is applied prior to the actual pulse sequence to compensate for sample heating occurring during the relaxation delay because of the application of 180° pulses. In all three pulse sequences an initial INEPT transfer is used which creates two coherence transfer pathways, $H_z \rightarrow 2C_xH_z$ and $C_z \rightarrow C_x$. The two pathways can be combined to enhance either the $C_+^{(\alpha)}$ or $C_+^{(\beta)}$ single transitions. The phase setting $\zeta' = +$y in sequences (A) and (B) enhances the narrow $C_+^{(\beta)}$ component, which is selected by the following S^{3}E filter sequence using $\chi = [x + 45^\circ]$, $\Psi_4 = [y, -y]$, and Rec = x. In sequence (C), the phase ζ is set to $\zeta = -$y for $C_+^{(\beta)}$ relaxation and to $\zeta = +$y for $C_+^{(\alpha)}$ relaxation measurement. For pulse schemes (A) and (B), quadrature detection in t_1 is obtained by time-proportional phase incrementation of Ψ_3 (initially set to $\Psi_3 =$ x) according to the hypercomplex method. For pulse scheme (C), two data sets E_1 and E_2 are recorded with the following phase settings: E_1: $\Psi_1 = [-x, x, -y, y]$, $\phi_1 = [y]$, $\Psi_2 = [x, x, -x, -x]$, Rec = [x, −x, y, −y], and E_2: $\Psi_1 = [-x, x, -y, y]$, $\phi_1 = [-y]$, $\Psi_2 = [-x, -x, x, x]$, Rec = [x, −x, y, −y]. Quadrature detection in t_1 is obtained by linear combination of the two data sets E_1 and E_2: *Real*(t_1) = $E_1 + E_2$ and *Imag*(t_1) = $E_1 - E_2$, and by an additional 90° phase shift of *Imag*(t_1) along the t_2(^{1}H) dimension.

This relaxation rate ratio can be used to probe variations of the ^{13}C CSA tensor or the C-H bond length along the nucleic acid chain.

In macromolecules the approximation of an isolated two-spin system is always questionable, as the presence of other spins offers multiple additional relaxation pathways. In order to evaluate the importance of such effects in RNA we have considered the ^{1}H-^{1}H dipolar interaction with an additional neighbouring spin. The auto-correlated relaxation rate constants $R(C_+)$ and $R(C_z)$, and the cross-correlated relaxation constant $\Gamma^{xy}_{C,CH}$ remain unaffected by the presence of an additional ^{1}H spin, while additional auto-relaxation ρ_{HH} and cross-relaxation σ_{HH} pathways for the antiphase coherence $2C_+H_z$ are introduced by the ^{1}H-^{1}H dipolar interaction. In the case of slowly tumbling molecules and neglecting internal motion, ρ_{HH} and σ_{HH} are equally efficient, $\rho_{HH} = -\sigma_{HH}$, and $R(C_+H_z)$ has to be replaced by an effective rate constant $R_{eff}(C_+H_z)$:

$$R_{eff}(C_+H_z) \cong R(C_+H_z) + \rho_{HH} \qquad (8)$$

The three-spin system is a reasonable approximation to the situation found in RNA where the proton density is much lower than in proteins (Wang et al., 1992; Liu et al., 1996). In the slow motion limit $\rho_{HH}/R(C_+H_z)$ becomes independent of the spectral density function, and the relative contribution of the ^{1}H-^{1}H interaction to the relaxation rate $R_{eff}(C_+H_z)$ is computed to be $\rho_{HH}/R(C_+H_z) \cong 0.04$ for $r_{HH} = 2.46$ Å and $\overline{\Delta\sigma} = 160$ ppm, corresponding to the H_5-H_6 distance and the C_6 CSA, respectively.

Materials and methods

The pulse sequences of Figures 1A and 1B are designed for the measurement of ^{13}C transverse $R(C_+)$ and longitudinal $R(C_z)$ relaxation rate constants, respectively. The common features of the two experiments are as follows: after an initial INEPT transfer step, spin-state selection is achieved by a slightly modified S^{3}E pulse scheme, which selects the slowly relaxing $C_x^{(\beta)}$ component. The following pulse sequence block filters signals originating from molecules with two adjacent ^{13}C carbons. During the filter delay Δ_{CC} relaxation occurs with the rate constant $R(C_+^{(\beta)})$ of the narrow doublet line, which minimises signal loss. The importance of such filter sequences (labelled as 'C-C filter') and their efficiency for the measurement of ^{13}C relaxation in fractionally labelled molecules will be discussed later. During the incremented time period t_1 the ^{13}C frequencies are edited while the ^{1}H spins remain in the favourable (β) spin state. Prior to the relaxation period, a filter is introduced which suppresses the antiphase coherence $2C_xH_z$. Such a preparation is necessary in order to avoid any admixture of in-phase and antiphase components during the relaxation delay. After the relaxation period a refocused ^{13}C-^{1}H INEPT sequence is used to create observable ^{1}H coherences for detection. During the spin-lattice relaxation period (Figure 1A) a train of 180° ^{1}H pulses suppresses cross-relaxation effects of C_z with $2C_zH_z$ and H_z due to the ^{1}H-^{13}C dipolar interaction and the CSA-dipolar cross-correlation (Kay et al., 1992). In the case of spin-spin relaxation (Figure 1B) the spin evolution is described by Equation 1. ^{13}C chemical shift and J_{CH} coupling evolution are refocused by application of a CPMG pulse train (Meiboom and Gill, 1958). The CSA-dipolar cross-correlation $\Gamma^{xy}_{C,CH}$ is suppressed by a ^{1}H 180° pulse train synchronised with the CPMG sequence (Kay et al., 1992).

The experiment of Figure 1C aims at measuring the relaxation rate constants of the individual lines of the ^{13}C (-^{1}H) doublet. The pulse scheme is derived from the TROSY sequence (Pervushin et al., 1997, 1998b; Brutscher et al., 1998). For the measurement of the $R(C_+^{(\alpha)})$ and $R(C_+^{(\beta)})$ rate constants, the same pulse sequence is used but with different phase settings as given in the caption of Figure 1. The relaxation period is included after the initial INEPT transfer. Depending on the relative phase of the following 90° ^{1}H pulses the single transition operators are either interchanged (α) $\longleftrightarrow$ (β) or not. This aims at keeping or restoring the slowly relaxing ^{13}C component $C_x^{(\beta)}$ for the following C-C filter sequence and the ^{13}C frequency editing during t_1. In the final transfer step the $C_x^{(\beta)}$ coherence is selected and transferred into an observable $H_x^{(\alpha)}$ coherence. As the orthogonal coherence $C_y^{(\beta)}$ is simultaneously transferred into a detectable coherence $H_y^{(\alpha)}$ this allows the application of the sensitivity enhancement scheme for quadrature detection in indirect frequency dimensions (Palmer et al., 1991). Several groups (Andersson et al., 1998; Brutscher et al., 1998; Pervushin et al., 1998a; Rance et al., 1999) have recently shown the applicability of sensitivity enhanced quadrature detection to TROSY. The antiphase part of the proton signal is suppressed by a phase cycled 90° ^{13}C pulse prior to detection and the application of a ^{13}C decoupling sequence (Cordier et al., 1999).

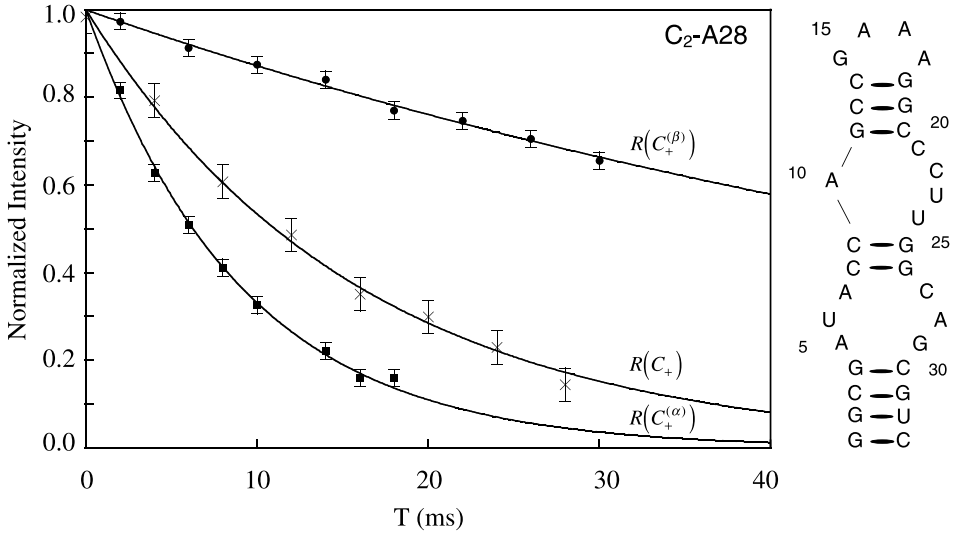

Figure 2. Experimental relaxation decay curves obtained for the C_2 carbon of nucleotide A28 in the 33-mer RNA–theophylline complex using the pulse sequences of Figure 1B for $R(C_+)$ and Figure 1C for $R(C_+^{(\alpha)})$ and $R(C_+^{(\beta)})$. All data were recorded using the same CPMG pulse train with an interpulse delay of $\tau_{CPMG} = 0.1$ ms. Filled circles and squares correspond to relaxation decays measured with the sequence of Figure 1C, the intermediate decay curve (×) was obtained with the sequence of Figure 1B. The secondary structure of the 33-mer RNA is drawn on the right.

As the ^{1}H CSA is small and consequently the CSA-dipolar cross-correlated relaxation is inefficient, this experimental procedure avoids small artefacts in the ^{1}H dimension due to the tuning of the TROSY transfer delays (Andersson et al., 1998; Brutscher et al., 1998) without loss of sensitivity. During the relaxation period T the spin evolution is described by Equation 2. The CPMG pulse sequence refocuses ^{13}C chemical shift evolution. No ^{1}H pulses are applied to avoid the mixture of (α) and (β) spin states during the relaxation delay. During the free spin evolution delays τ_{CPMG}, the large J_{CH} couplings ($J_{CH} \approx 190$ Hz for base carbons) ensure mono-exponential relaxation of the two ^{13}C doublet lines.

Different experimental techniques (S^3E or TROSY) are used for spin-state selection in the sequences of Figures 1A & B and Figure 1C, respectively. In the TROSY sequence spin-state selection is achieved during the final $^{13}C \rightarrow {}^1H$ transfer step, whereas the S^3E pulse scheme can be inserted at any place in the pulse sequence. In general TROSY is preferred, as sensitivity enhanced quadrature detection and spin-state selection are concatenated with the final $^{13}C \rightarrow {}^1H$ transfer step. In the case of the S^3E sequence, additional relaxation occurs during the delay of $\Delta_{CH}/2$, where the spin system relaxes at the average rate constant $\overline{R_+}$. In the experiments of Figures 1A and B the S^3E technique was applied before cancellation of the antiphase coherence $2C_zH_z$ to conserve the benefit of using both ^{1}H and ^{13}C steady-state polarisations. The C-C filter and the t_1 frequency editing in these experiments have to be placed before the relaxation period in order to take advantage of the favourable relaxation properties of the $C_+^{(\beta)}$ coherence.

All experiments are demonstrated on a 33-mer RNA in a 1:1 complex with unlabelled theophylline (Zimmermann et al., 1997). Theophylline is a bronchodilator, chemically analogous to caffeine with a molecular weight of 180 Da (Jenison et al., 1994). The RNA was 15% ^{13}C labelled and dissolved in a buffer of 20 mM sodium phosphate (pH 6.8), 30 mM NaCl, 2 mM $mgCl_2$ in D_2O at a sample concentration of about 1 mM. Theophylline was then added to the solution to form a 1:1 complex with the RNA. Data were recorded on a Varian INOVA 600 MHz spectrometer at a sample temperature of 298 K. Data processing was achieved using the FELIX program version 97.0 (Molecular Simulations Inc.).

Two-dimensional ^{1}H-^{13}C correlation spectra were acquired using the experiments of Figure 1 with 512 (^{1}H) × 256 (^{13}C) complex points and spectral widths of 7804 and 9054 Hz, respectively. The carrier frequencies were set on the water resonance (4.7 ppm) for ^{1}H and the centre of the C_2, C_6, and C_8 base carbons (147 ppm) for ^{13}C. The CPMG pulse train was carefully calibrated at a power level of $|\gamma B_1|/2\pi =$

19 kHz and the effectively refocused frequency bandwidth was experimentally determined on a 1% ^{13}C-labelled iodomethane sample to be ±4000 Hz. The relaxation decays were sampled at eight time points: 40, 80, 160, 260, 400, 600, 800, 1000 ms for $R(C_z)$; 0, 4, 8, 12, 16, 20, 24, 28 ms for $R(C_+)$; 2, 4, 6, 8, 10, 14, 16, 18 ms for $R(C_+^{(\alpha)})$; and 2, 6, 10, 14, 18, 22, 26, 30 ms for $R(C_+^{(\beta)})$. The overall experimental time was about four days per relaxation series. All spectra were processed using two different protocols to optimise either signal-to-noise or resolution of the cross peaks. In both cases a Lorentzian to Gaussian apodization was applied in ω_2(^{1}H), whereas in the ω_1(^{13}C) dimension a squared cosine function was used, shifted by 30° for resolution enhancement. The data were zero-filled, multiplied with the apodization function and Fourier transformed yielding final matrices of 8192 × 8192 data points. The spectra were baseline corrected in both dimensions using the FLATT algorithm (Dietrich et al., 1991). Peak intensities were extracted from the 2D spectra using a local grid search routine for each cross peak. Uncertainties in measured peak heights were estimated from the spectral noise level and from recording the same experiment twice. A good qualitative agreement between these two measurements was obtained. The relaxation rate constants $R_i(R(C_z), R(C_+), R(C_+^{(\alpha)}), R(C_+^{(\beta)}))$ were determined by fitting the measured peak heights to a two-parameter function of the form $I(T) = I_0 \exp(-R_i T)$, where $I(T)$ is the intensity after a delay time T and I_0 is the intensity at $T = 0$.

The cross-correlated relaxation rate constant $\Gamma^{xy}_{C,CH}$ and the average auto-correlated rate constant $\overline{R_+}$ were then calculated as $\Gamma^{xy}_{C,CH} = \frac{1}{2}(R(C_+^{(\alpha)}) - R(C_+^{(\beta)}))$ and $\overline{R_+} = \frac{1}{2}(R(C_+^{(\alpha)}) + R(C_+^{(\beta)}))$, respectively.

Results and discussion

Well-resolved ^{1}H-^{13}C correlation maps of the base region of the RNA in the theophylline complex were obtained (Brutscher et al., 1998) with the pulse sequences of Figure 1 and relaxation data for 7 C_2, 8 C_6, and 11 C_8 sites could be extracted. Additional $R(C_z)$ rate constants were measured for 10 C_5 carbon sites. Typical relaxation decay curves obtained for the C_2 carbon of nucleotide A28 are shown in Figure 2: the intermediate curve corresponds to the relaxation decay of the C_+ coherence measured with the S^{3}E-based pulse sequence of Figure 1B and the upper and lower curves to the relaxation decays of the individual doublet components $C_+^{(\alpha)}$ and $C_+^{(\beta)}$ obtained with the TROSY-based sequence of Figure 1C. Note the larger error bars of the cross-peak intensities for the C_+ measurements. This difference is due to the inherent sensitivity of the two pulse sequences of Figures 1B and C as explained above. In the case of the CPMG relaxation experiments only the C_2, C_6, and C_8 cross peaks were used for a quantitative analysis because of the limited frequency bandwidth covered by the CPMG pulse train. The measured $R(C_z)$ and $R(C_+)$ rate constants for the C_2, C_6, and C_8 base carbons are displayed in Figures 3A and 3B, respectively.

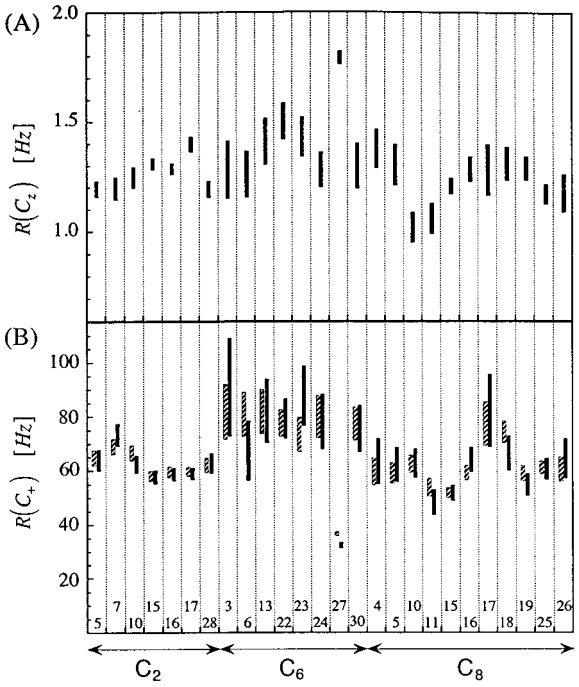

Figure 3. ^{13}C relaxation data measured for the C_2, C_6, and C_8 carbons in the 33-mer RNA–theophylline complex. In (A) are plotted the $R(C_z)$ values obtained with the pulse sequence of Figure 1A, in (B) the $R(C_+)$ rate constants measured with the pulse sequence of Figure 1B (dark bars) or Figure 1C (dashed bars). In both cases the interpulse delay τ_{CPMG} was set to 1.0 ms.

In Figure 3B the transverse relaxation rate constants $R(C_+)$ obtained with the sequence of Figure 1B (dark bars) are compared to relaxation rates measured with the sequence of Figure 1C (dashed bars). For the latter, two independent series of experiments have been carried out for measuring the $R(C_+^{(\alpha)})$ and $R(C_+^{(\beta)})$ relaxation rate constants and the reported values correspond to their average $\overline{R_+}$. The two rate con-

stants are identical within the experimental errors. The good experimental agreement clearly demonstrates the validity of the two-spin approximation for the majority of ^{13}C-^{1}H sites in our RNA molecule. It shows that the ^{1}H-^{1}H dipolar contributions in Equation 8 are small compared to the ^{13}C relaxation rate constant: $\rho_{HH} \ll R(C_+H_z)$ and $\sigma_{HH} \ll R(C_+H_z)$, and confirms the assumption that the power spectral density at the proton frequency $J(\omega_H)$ is small compared to $J(0)$ and $J(\omega_C)$. One can therefore safely neglect the $J(\omega_H)$ term in Equation 4 and obtain the following relation:

$$\overline{R_+} \cong (R(C_+H_z) + R(C_+))/2 \cong R(C_+) \qquad (9)$$

One exception is the C_6 carbon of C27, where the measured rate constants $R(C_+)$ and $\overline{R_+}$ differ by 3 s^{-1} (≈10% of the absolute value). According to the structural studies of the 33-mer RNA bound to theophylline (Zimmermann et al., 1997), C27 is not involved in any base pairing with other nucleotides and the base points towards the outside of the complex. The high degree of internal flexibility was previously observed by Zimmermann et al. (1998) and is also confirmed by the large $R(C_z)$ and small $R(C_+)$ rate constants measured in our present study (Figures 3A and B). Therefore it is not surprising that the two measurements yield slightly different results. Nevertheless, even for this highly flexible nucleotide the $\overline{R_+}$ rate constant provides a good estimate for $R(C_+)$.

The TROSY-based pulse scheme of Figure 1C thus allows simultaneous measurement of the cross-correlated relaxation rate constant $\Gamma^{xy}_{C,CH}$, and of the rate constant $\overline{R_+}$, which to a good approximation is identical to $R(C_+)$ (Equation 9) and therefore contains additional useful information on molecular motion.

C-C filter efficiency and optimal ^{13}C enrichment

In a 15% randomly ^{13}C-enriched RNA, the signal intensity originating from isolated ^{13}C (^{1}H) systems (singlet peaks) is expected to be 15 times higher than in the case of a natural abundance sample. However, in the presence of adjacent carbons as in the case of C_6 and C_5 in pyrimidine bases, additional scalar and dipolar ^{13}C-^{13}C interactions have to be taken into account. The dipolar interactions offer additional relaxation pathways, whereas the scalar couplings create an oscillatory contribution during the transverse relaxation decay. In the case of C_6 and C_5 base carbons, the contribution originating from the ^{13}C-^{13}C isotopomers to the detected signal is 15% and 30%, respectively. These non-negligible signals appear in the spectrum as additional unresolved or poorly resolved doublet peaks with a splitting of $^{1}J_{CC} \cong 67$ Hz, centred around the predominant singlet peak. This peak overlap prevents the accurate measurement of the singlet peak intensities. Reliable relaxation measurement for these sites requires filtering of unwanted signals due to the ^{13}C-^{13}C pairs. C-C filters (Wand et al., 1995) have been implemented in the three pulse sequences depicted in Figure 1. In principle, the position of the C-C filter (and of the t_1 evolution period) in the pulse sequence can be freely swapped but sensitivity dictates that it should be applied when the spin system relaxes with the favourable $R(C_+^{(\beta)})$ rate constant. All data recorded with the sequences of Figures 1B and 1C showed a mono-exponential relaxation decay. This was not the case for the C_6 carbons when the spectra were recorded without a C-C filter inserted in the pulse sequences (data not shown). During the additional time required for the filter, there is a concomitant loss of sensitivity due to relaxation. This signal loss is considerably reduced by the use of spin-state selective techniques. On the basis of the measured relaxation rate constants on our 33-mer RNA sample a signal gain ranging from 30 to 50% with respect to standard (non-spin-state selective) filter techniques can be computed assuming an exponential decay of the magnetisation during the required filter delay of $\Delta_{CC} = 7.5$ ms. On an absolute scale the implementation of the C-C filter is accompanied by a loss of only 10 to 20%. These data can be extrapolated for the case of larger RNA molecules with tumbling correlation times of $\tau = 20$ and 30 ns, yielding a relative signal gain of a factor of 2 and 3, respectively. Even for such large RNA molecules the absolute signal loss due to the filter would be limited to about 40% (instead of 75%) using spin-state selective techniques. Note that in the case of pyrimidine C_5 the triplet signals originating from the $^{13}C_6$-$^{13}C_5$-$^{13}C_4$ isotopomer are not suppressed by the C-C filter, but at low levels of ^{13}C enrichment they can be safely neglected (≈3% in the present case).

As the different sites in an RNA molecule have either no, one or two carbon neighbours, the optimal level of random fractional labelling will be different for each site. Neglecting long-range carbon-carbon interactions and requiring a negligible contribution from the unsuppressed $^{13}C_6$-$^{13}C_5$-$^{13}C_4$ isotopomer it appears that the optimal isotopic enrichment would have been 100% for C_2 and C_8, 50% for C_6 (and $C_{1'}$, $C_{5'}$ sugar carbons) and 25% for C_5 (and $C_{2'}$, $C_{3'}$, and $C_{4'}$

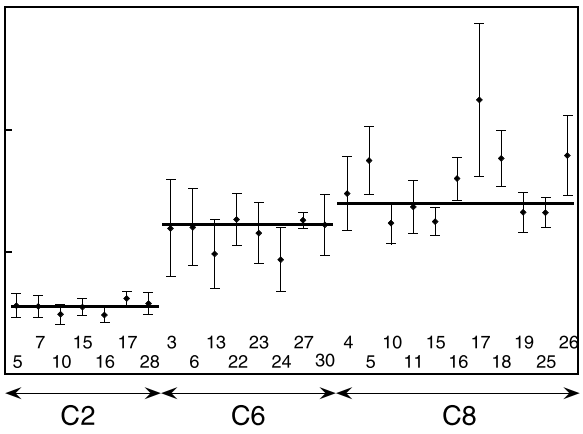

Figure 4. $R(C_+)/\Gamma^{xy}_{C,CH}$ ratios obtained for the C_2, C_6, and C_8 carbons in the 33-mer RNA–theophylline complex. The two rate constants were measured with the pulse sequence of Figure 1C. The delay between successive 180° pulses in the CPMG sequence was kept short, $\tau_{CPMG} = 0.1$ ms, to suppress conformational exchange contributions to $R(C_+)$. Horizontal lines correspond to calculated mean values: 1.28 ± 0.01 for C_2, 1.61 ± 0.03 for C_6 and 1.70 ± 0.03 for C_8.

sugar carbons). For a 25% ^{13}C-labelled sample the signal intensity of the central line of the triplet peak is about 5% of the singlet peak. In conclusion, a 25% randomly ^{13}C-labelled sample appears to be a good compromise for the study of local molecular dynamics in RNA at a large number of carbon sites.

Chemical shift anisotropy of base carbons

Chemical shift anisotropy of base carbons in nucleic acids is a major source of ^{13}C relaxation at high magnetic field strengths. For the interpretation of the measured relaxation data in terms of molecular dynamics, the accurate knowledge of ^{13}C CSA tensors in nucleic acids is therefore a prerequisite. At this time no experimental CSA data are available for carbons in purine or pyrimidine bases. In a recent review, Sitkoff and Case (1998) reported Density Functional Theory (DFT) calculations of ^{13}C CSA tensors in 9-methyl-purine and 1-methyl-pyrimidine. The DFT calculations and solid state NMR measurements on benzene derivatives (Veeman, 1984) confirm that the CSA tensor is fully anisotropic with one principal axis orthogonal to the aromatic ring and a second approximately parallel to the C-H bond (with a deviation of 0°–20°). While the orientations are almost conserved among these systems, large variations in the CSA magnitude have been reported.

CSA tensor information can also be obtained from liquid state NMR relaxation measurements. In Figure 4 $R(C_+)/\Gamma^{xy}_{C,CH}$ ratios measured for the C_2, C_6, and C_8 positions of our 33-mer RNA are shown. This ratio is to a first approximation independent of molecular motion (Equation 7) and therefore different ratios reflect either variations in the CSA tensor or the local molecular geometry.

The $R(C_+)/\Gamma^{xy}_{C,CH}$ ratios obtained for the C_2 carbons of adenine, which have the smallest experimental errors, are remarkably constant. In the case of the C_6 and C_8 carbons the interpretation of the data is complicated by the relatively large errors. Assuming no variation of the C-H bond distance and thus a constant value for ξ_{DD}, a few conclusions can be drawn from this figure: (i) the assumption of isotropic motion and negligible high frequency contributions to the spectral density function seems to be relatively well satisfied in the present case; (ii) the mean values for the $R(C_+)/\Gamma^{xy}_{C,CH}$ ratios vary considerably between the chemically different carbons: 1.28 ± 0.01 for C_2, 1.61 ± 0.03 for C_6, and 1.70 ± 0.03 for C_8. This clearly indicates that contrary to previous studies on RNA and DNA systems different CSA tensors have to be taken into account for the analysis of ^{13}C relaxation data for different types of carbon; (iii) the variations from one base to another for a given carbon type (C_2, C_6, C_8) are small compared to the differences between them. The most outlying $R(C_+)/\Gamma^{xy}_{C,CH}$ ratio corresponds to C_8 of nucleotide A17, which undergoes important conformational exchange, as will be shown in the next section. The pulse repetition rate of the CPMG sequence ($\tau_{CPMG} = 0.1$ ms) is apparently too slow to completely suppress the R_{ex} contribution to $R(C_+)$ for this spin.

Finally, our experimental results can be compared to the DFT calculations of Sitkoff and Case (1997). As expected for isolated bases the calculated CSA tensors differ for unlike carbon types, but only minor variations are reported for the C_8 carbons in adenine and guanine, or the C_6 and C_5 carbons in cytidine and uridine. The $R(C_+)/\Gamma^{xy}_{C,CH}$ ratios calculated with Equation 7 on the basis of the reported CSA tensors and setting the aromatic C-H distance to $r_{C\text{-}H} = 1.08$ Å (Allen et al., 1987) are: 1.31 for C_2, 1.35 for C_6, and 1.61 for C_8. The calculated ratios for the C_2 and C_8 carbon sites are very close to the experimentally determined values for these carbon types. In the case of C_6 the calculated CSA tensors cannot accurately reproduce the experimental data, indicating that the influence of the ribose ring may not be correctly taken into account by the methyl group replacement. Both DFT calculations and NMR relaxation measure-

ments show that ^{13}C CSA are smaller in RNA bases than in most benzene and toluene derivatives (Veeman, 1984), which have until now often been used as model systems for the analysis of ^{13}C spin relaxation data in RNA.

A more detailed picture of the ^{13}C CSA tensors in RNA from NMR relaxation data will be obtained from measurements at different magnetic fields (Fushman et al., 1998). The B_0 field dependence of the $R(C_+)/\Gamma^{xy}_{C,CH}$ ratios allows the separation of the two relevant relaxation CSA parameters $\overline{\Delta\sigma}$ and $\Delta\sigma^*$ using the analytical expression given in Equation 7. This work is currently in progress in our laboratory.

Detection of conformational exchange processes

Conformational and chemical exchange processes on the microsecond to millisecond time scale are manifest as an additional contribution R_{ex} to the spin-spin relaxation rate constants (Equations 3 and 4). For ^{15}N relaxation data in the protein backbone it has been recently shown (Brutscher et al., 1997; Kroenke et al., 1998) that a comparison of the cross-correlated relaxation rate constants $\Gamma^{xy}_{C,CH}$ and the auto-correlated rate constants $R(C_+)$ allows the identification of exchange processes. Assuming isotropic motion and identical CSA tensors for the different ^{13}C sites, these two parameters $\Gamma^{xy}_{C,CH}$ depend in a similar way on the spectral density function $J(\omega)$ (Equations 4 and 5), except that conformational exchange does not contribute in the case of $\Gamma^{xy}_{C,CH}$. In the present study only the C_8 of nucleotide A17 could be unambiguously identified as experiencing conformational exchange when comparing the two relaxation rate constants obtained with the sequence of Figure 1C and a CPMG delay of $\tau_{CPMG} = 2.0$ ms (data not shown). While this comparison represents a simple and generally applicable method for the identification of larger exchange contributions, it will not distinguish between small R_{ex} terms and anisotropic motions or variations in the ^{13}C CSA tensor.

More quantitative information concerning the exchange contributions can be obtained from relaxation data recorded at multiple B_0 field strengths (Peng and Wagner, 1995; Phan et al., 1996), off-resonance rotating-frame spin relaxation experiments (Deverell et al., 1970; Akke and Palmer, 1996), or from variation of the pulse spacing within the CPMG pulse train. Here we will focus on exchange processes revealed by CPMG transverse relaxation experiments. Bloom et al. (1955) have computed the exchange contribution R_{ex} for a two-step process during a CPMG pulse train:

$$R_{ex} = (\delta\omega)^2 p_A p_B \tau_{ex} \left\{ 1 - \frac{\tau_{ex}}{\tau_{CPMG}} \tanh\left(\frac{\tau_{CPMG}}{\tau_{ex}} \right) \right\} \quad (10)$$

where τ_{CPMG} is the delay between the 180° pulses in the CPMG pulse train; p_A and p_B are the populations of the two exchanging states; $\delta\omega$ is the chemical shift difference between the two substates, and τ_{ex} is the characteristic time constant of the exchange process. Equation 10 implies that the R_{ex} contributions are completely suppressed when the spacing of the 180° pulses is much smaller than the exchange time constant, $\tau_{CPMG} \ll \tau_{ex}$.

In order to experimentally detect exchange contributions R_{ex}, the relaxation experiments are repeated several times, varying τ_{CPMG}. In standard ^{13}C relaxation experiments R_{ex} is estimated from the τ_{CPMG}-dependence of $R(C_+)$ rate constants. The accuracy of the measurement, however, becomes quite poor if R_{ex} is much smaller than $R(C_+)$, as the exchange term is obtained from the difference of two large but close values, $R(C_+)$ and $(R(C_+)+R_{ex})$. Spin-state selective techniques again offer the possibility to increase the sensitivity of the conformational exchange measurements, by monitoring the effect on the slowly relaxing $C_+^{(\beta)}$ coherence, which is affected in the same way by the exchange process as C_+. Ishima et al. (1998) have recently proposed a similar approach for measuring exchange contributions to amide proton spin-spin relaxation rate constants of proteins. As dipolar and CSA contributions to $C_+^{(\beta)}$ relaxation are independent of τ_{CPMG} (Equation 2), the pulse sequence of Figure 1C allows the use of long τ_{CPMG} (several milliseconds) without modification of the CPMG sequence. This presents an attractive alternative to the recently introduced technique of Loria et al. (1999), where an additional pulse element is introduced to interconvert in-phase C_+ and antiphase coherences $2C_+H_z$ during τ_{CPMG}.

In Figure 5 two examples of carbon sites undergoing measurable conformational exchange are shown. The relaxation decays were obtained by recording experiments with the pulse sequence of Figure 1C with phase adjustment for $C_+^{(\beta)}$ relaxation using two different CPMG pulse trains: $\tau_{CPMG} = 0.1$ ms and $\tau_{CPMG} = 2.0$ ms. Note that even for the short τ_{CPMG} delays, a mono-exponential decay of the relaxation curves is obtained. As discussed previously, this observation reflects the fact that $\Gamma^{xy}_{C,CH} \gg \Delta R_+$ (Equation 2). In the case of C_8 of nucleotide A17,

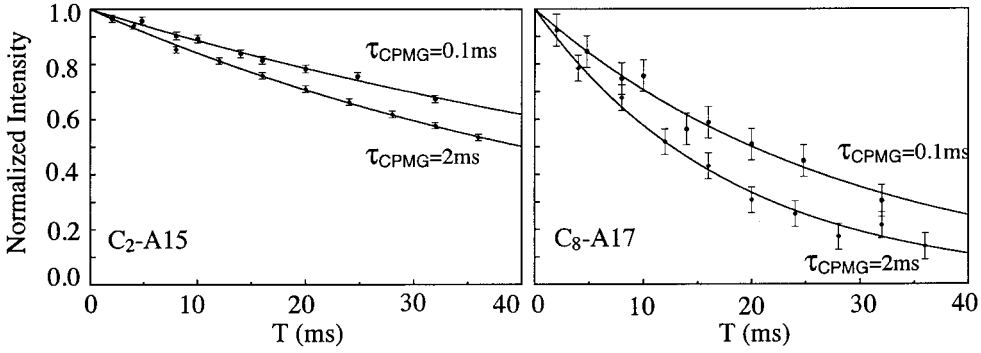

Figure 5. $C_+^{(\beta)}$ relaxation decay curves obtained for C_2 of nucleotide A15 (left part) and C_8 of nucleotide A17 (right part), both located in a GA_3 loop region of the RNA. The relaxation data were recorded with the pulse sequence of Figure 1C using different CPMG delays: $\tau_{CPMG} = 0.1$ ms (circles) and $\tau_{CPMG} = 2.0$ ms (diamonds). Differences in the relaxation decay curves for the two CPMG delays reflect the presence of conformational exchange processes for the two nuclei: $R_{ex} \cong 5.2\ s^{-1}$ for C_2-A15, and $R_{ex} \cong 20\ s^{-1}$ for C_8-A17.

an exchange contribution of $R_{ex} \cong 20\ s^{-1}$ is obtained, whereas in the case of the C_2 of A15 a small exchange effect $R_{ex} \cong 5.2\ s^{-1}$ is clearly identified from the two relaxation curves. This small exchange effect of C_2 of A15 would have been difficult to detect from the τ_{CPMG} dependence of the fast relaxing C_+ coherence. Both nucleotides A15 and A17 are located in a GA_3 loop region of the RNA (see Figure 2). Conformational exchange processes in GA_3 hairpin loops have previously been identified (Legault and Pardi, 1994). GA_3 loops are frequently found in biological RNA and are reported to be involved in molecular recognition and complexation (Cate et al., 1996; Legault et al., 1998). The above described relaxation experiment provides a sensitive method for the localisation of internal motions on the micro- to millisecond time scale in RNA, which is important for the understanding of biological mechanisms.

Conclusions

We have shown that spin-state selective correlation techniques provide a powerful tool for the study of ^{13}C spin relaxation in RNA bases, as they significantly increase the sensitivity and spectral resolution of the NMR experiments. Fractional ^{13}C-labelling and inclusion of C-C filters in the pulse sequences ensure a mono-exponential relaxation decay and allow the further interpretation of the relaxation data in terms of molecular motion sampled at the different ^{13}C-^1H sites in the RNA. Signal loss during the C-C filter delay is minimised by exploiting the favourable relaxation properties of the slowly relaxing $C_+^{(\beta)}$ doublet component. The presented experiments will be equally useful for the study of molecular dynamics in fractionally ^{13}C-labelled DNA. A preliminary analysis of the measured relaxation rate constants in a 33-mer RNA showed significant variations in the ^{13}C CSA tensor from one carbon type to another. As a consequence, carbon-type dependent CSA tensors will be necessary for the accurate interpretation of RNA relaxation data in terms of molecular dynamics. The detection of small conformational exchange effects by a sensitive experimental technique provides evidence for local motion on the micro- to millisecond time scale in the GA_3 loop region of the RNA.

Acknowledgements

We thank Art Pardi, Grant Zimmermann and Analisa Brown for providing the 15% ^{13}C-labelled RNA–theopylline complex. This work was supported by the Commissariat à l'Energie Atomique, the Centre National de la Recherche Scientifique, and Molecular Simulations Inc. (San Diego, CA). This is publication no. 629 of the Institut de Biologie Structurale Jean-Pierre Ebel.

References

Akke, M. and Palmer III, A.G. (1996) *J. Am. Chem. Soc.*, **118**, 911–912.

Akke, M., Fiala, R., Jiang, F., Patel, D. and Palmer III, A.G. (1997) *RNA*, **3**, 702–709.

Allen, F.H., Kennard, O., Watson, D.G., Brammer, L., Orpen, A.G. and Taylor, R. (1987) *J. Chem. Soc. Perkin. Trans.* II, S1–S19.

Andersson, P., Annila, A. and Otting, G. (1998) *J. Magn. Reson.*, **133**, 364–367.

Bloom, M., Reeves, L.W. and Wells, E.J. (1965) *J. Chem. Phys.*, **42**, 1615–1624.
Borer, P.N., LaPlante, S.R., Kumar, A., Zanatta, N., Martin, A., Hakkinen, A. and Levy, G.C. (1994) *Biochemistry*, **33**, 2441–2450.
Brutscher, B., Brüschweiler, R. and Ernst, R.R. (1997) *Biochemistry*, **36**, 13043–13053.
Brutscher, B., Boisbouvier, J., Pardi, A., Marion, D. and Simorre, J.-P. (1998) *J. Am. Chem. Soc.*, **120**, 11845–11851.
Cate, J.H., Gooding, A.R., Podell, E., Zhou, K., Golden, B.L., Kundrot, C.E., Cech, T.R. and Doudna, J.A. (1996) *Science*, **273**, 1678–1685.
Cavanagh, J., Fairbrother, W.J., Palmer III, A.G. and Skelton, N.J. (1996) *Protein NMR Spectroscopy*, Academic Press Inc., San Diego, CA.
Cordier, F., Dingley, A.J. and Grzesiek, S. (1999) *J. Biomol. NMR*, **13**, 175–180.
Deverell, C., Morgan, R.E. and Strange, J.H. (1970) *Mol. Phys.*, **4**, 553–559.
Dietrich, W., Rüdel, C.H. and Neumann, M. (1991) *J. Magn. Reson.*, **91**, 1–11.
Fushman, D. and Cowburn, D. (1998) *J. Am. Chem. Soc.*, **120**, 7109–7110.
Fushman, D., Tjandra, N. and Cowburn, D. (1998) *J. Am. Chem. Soc.*, **120**, 10947–10952.
Goldman, M. (1984) *J. Magn. Reson.*, **60**, 437–452.
Ishima, R., Wingfield, P.T., Stahl, S.J., Kaufman, J.D. and Torchia, D.A. (1998) *J. Am. Chem. Soc.*, **120**, 10534–10542.
Jenison, R.D., Gill, S.C., Pardi, A. and Polisky, B. (1994) *Science*, **263**, 1425–1429.
Kay, L.E., Torchia, D.A. and Bax, A. (1989) *Biochemistry*, **28**, 8972–8979.
Kay, L.E., Nicholson, L.K., Delaglio, F., Bax, A. and Torchia, D.A. (1992) *J. Magn. Reson.*, **97**, 359–375.
Kojima, C., Ono, A., Kainosho, M. and James, T.L. (1998) *J. Magn. Reson.*, **135**, 310–333.
Kroenke, C.D., Loria, J.P., Lee, L.K., Rance, M. and Palmer III, A.G. (1998) *J. Am. Chem. Soc.*, **120**, 7905–7915.
Legault, P. and Pardi, A. (1994) *J. Magn. Reson.*, **B103**, 82–86.
Legault, P., Li, J., Mogridge, J., Kay, L.E. and Greenblatt, J. (1998) *Cell*, **93**, 289–299.
Liu, H., Tonelli, M. and James, T. L. (1996) *J. Magn. Reson.*, **B111**, 85–89.
Loria, J.P., Rance, M. and Palmer III, A.G. (1999) *J. Am. Chem. Soc.*, **121**, 2331–2332.
Meiboom, S. and Gill, D. (1958) *Rev. Sci. Instrum.*, **29**, 688–691.
Meissner, A., Duus, J.Ø. and Sørensen, O.W. (1997) *J. Magn. Reson.*, **128**, 92–97.
Ottiger, M., Delaglio, F. and Bax, A. (1998) *J. Magn. Reson.*, **131**, 373–378.
Palmer III, A.G., Cavanagh, J., Wright, P. and Rance, M. (1991) *J. Magn. Reson.*, **93**, 151–170.
Paquet, F., Gaudin, F. and Lancelot, G. (1996) *J. Biomol. NMR*, **8**, 252–260.
Peng, J.W. and Wagner, G. (1995) *Biochemistry*, **34**, 16733–16752.
Pervushin, K., Riek, R., Wider, G. and Wüthrich, K. (1997) *Proc. Natl. Acad. Sci. USA*, **94**, 12366–12371.
Pervushin, K., Wider, G. and Wüthrich, K. (1998a) *J. Biomol. NMR*, **12**, 345–348.
Pervushin, K., Riek, R., Wider, G. and Wüthrich, K. (1998b) *J. Am. Chem. Soc.*, **120**, 6394–6400.
Phan, I.Q.H., Boyd, J. and Campbell, I.D. (1996) *J. Biomol. NMR*, **8**, 369–378.
Rance, M., Loria, J.P. and Palmer III, A.G. (1999) *J. Magn. Reson.*, **136**, 92–101.
Shaka, A.J., Freeman, R. and Barker, P.B. (1985) *J. Magn. Reson.*, **64**, 547–552.
Sitkoff, D. and Case, D. (1998) *Prog. NMR Spectr.*, **32**, 165–190.
Spielmann, H.P. (1998) *Biochemistry*, **37**, 16863–16876.
Veeman, W. (1984) *Prog. NMR Spectrosc.*, **16**, 193–235.
Wand, A.J., Bieber, R.J., Urbauer, J.L., McEvoy, R.P. and Gan, Z. (1995) *J. Magn. Reson.*, **B108**, 173–175.
Wang, A.C., Kim, S.G., Flynn, P., Chou, S.H., Orban, J. and Reid, B. (1992) *Biochemistry*, **31**, 3940–3946.
Williamson, J.R. and Boxer, S.G. (1989) *Biochemistry*, **28**, 2819–2831.
Yamazaki, T., Muhandiram, R. and Kay, L.E. (1994) *J. Am. Chem. Soc.*, **116**, 8266–8278.
Zimmermann, G.R., Jenison, R.D., Wick, C.L., Simorre, J.-P. and Pardi, A. (1997) *Nat. Struct. Biol.*, **4**, 644–649.
Zimmermann, G.R., Shields, T.P., Jenison, R.D., Wick, C.L. and Pardi, A. (1998) *Biochemistry*, **37**, 9186–9192.